

This article was downloaded by: [University of California, Berkeley]

On: 25 March 2010

Access details: Access Details: [subscription number 915549789]

Publisher Taylor & Francis

Informa Ltd Registered in England and Wales Registered Number: 1072954 Registered office: Mortimer House, 37-41 Mortimer Street, London W1T 3JH, UK



Journal of Earthquake Engineering

Publication details, including instructions for authors and subscription information:

<http://www.informaworld.com/smpp/title~content=t741771161>

Lessons Learned from Seismic Analysis of a Seven-Story Concrete Test Building

Jonathan D. Waugh^a; Sri Sritharan^a

^a Department of Civil, Construction, and Environmental Engineering, Iowa State University, Ames, Iowa, USA

Online publication date: 01 March 2010

To cite this Article Waugh, Jonathan D. and Sritharan, Sri (2010) 'Lessons Learned from Seismic Analysis of a Seven-Story Concrete Test Building', Journal of Earthquake Engineering, 14: 3, 448 – 469

To link to this Article: DOI: 10.1080/13632460903206485

URL: <http://dx.doi.org/10.1080/13632460903206485>

PLEASE SCROLL DOWN FOR ARTICLE

Full terms and conditions of use: <http://www.informaworld.com/terms-and-conditions-of-access.pdf>

This article may be used for research, teaching and private study purposes. Any substantial or systematic reproduction, re-distribution, re-selling, loan or sub-licensing, systematic supply or distribution in any form to anyone is expressly forbidden.

The publisher does not give any warranty express or implied or make any representation that the contents will be complete or accurate or up to date. The accuracy of any instructions, formulae and drug doses should be independently verified with primary sources. The publisher shall not be liable for any loss, actions, claims, proceedings, demand or costs or damages whatsoever or howsoever caused arising directly or indirectly in connection with or arising out of the use of this material.

Lessons Learned from Seismic Analysis of a Seven-Story Concrete Test Building

JONATHAN D. WAUGH and SRI SRITHARAN

Department of Civil, Construction, and Environmental Engineering, Iowa State University, Ames, Iowa, USA

A uniaxial shake table test of a full-scale slice of a seven-story reinforced concrete wall building was performed at the University of California, San Diego. A 2D analytical model that primarily employed fiber-based beam-column elements was used for a blind prediction of the global response of the building to the imposed input accelerations. An improved analytical model, which adequately simulates the building's dynamic response and comparison of measured and analytical results, is presented. The lessons learned from participation in the blind prediction with particular attention to the effects of issues commonly ignored in analytical modeling of concrete buildings are included.

Keywords Concrete; Wall; Multi-story Building; Shake Table Testing; Seismic; Dynamic; Analysis; Nonlinear

1. Introduction

In the fall of 2005, a portion of a full-scale seven-story concrete building, which is hereafter referred to as the test building, was constructed and tested under unidirectional earthquake motions using an outdoor shake table at the University of California, San Diego (UCSD). A capacity-based design approach was used to determine the structural details of the building elements, which led to smaller member dimensions and reduced amounts of reinforcing steel than those typically required by a traditional design code approach [Restrepo, 2006]. The smaller member sizes and reduced reinforcing steel created a more flexible structure that was both economical and easier to construct, while satisfying criteria to produce ductile response for the building under the selected seismic input motions.

A blind prediction contest was held from April to May 2006, in which teams of practicing engineers, researchers, and students from all over the world participated and predicted the expected response of the test structure using the construction details and measured engineering material properties made available to them. The time-histories of the four input motions, named EQ1, EQ2, EQ3, and EQ4, were also provided as part of the contest. The model used for the blind prediction by the writers, hereafter referred to as the original model, was developed based on fiber-based beam column elements available in OpenSees [Mazzoni *et al.*, 2004]. Other participants used various modeling approaches including: 3D solid elements, plain stress elements, multiple vertical line elements, and elastic beam elements [Restrepo, 2006]. The original model under predicted the overturning moments by 30–40%, story shear forces by 20–40%, and the residual displacements by 50–70%. The lateral displacement envelope was adequately predicted for EQ1

Received 10 December 2007; accepted 22 July 2009.

Address correspondence to Sri Sritharan, Department of Civil, Construction, and Environmental Engineering, Iowa State University, 394 Town Engineering Building, Ames, IA 50011, USA; E-mail: sri@iastate.edu

and EQ3, and under predicted for EQ2 and EQ4. In general, the floor accelerations were the best predicted quantities for events EQ1, EQ2, and EQ3, where the original model predicted values within 20% of the recorded floor accelerations of the test building. For EQ4, the floor accelerations were over predicted by 20–35%. The response of the building to EQ3, particularly the overturning moments, was difficult for participants to capture [Restrepo, 2006; Trevor, 2007]. A full description and discussion of the original model and corresponding results can be found in Waugh and Sritharan [2006].

A number of components were responsible for the discrepancies between the results from the original model and the recorded test data. The components that were ignored in the original model were the couple generated by the gravity columns, the stiffening effect of the link slab, and the flexibility of the shake table and foundation. Most of the participants made similar decisions about the importance of modeling these portions of the structure, as reported in the articles found in the proceedings of the NEES/UCSD Workshop on the Analytical Modeling of Reinforced Concrete Walls [Restrepo, 2006]. However, the excluded structural elements played an important role in the overall response, and thus influenced the accuracy of the predicted response parameters. Additionally, the structure had limited non structural elements, which in general significantly contribute to viscous damping, causing most of the analytical models to experience an excessive amount of viscous damping.

In this article, an improved analytical model is presented by addressing the shortcomings of the original model. This model, hereafter referred to as the improved model, builds on the strengths of the original model and includes additional important features that are typically ignored when modeling multi-story buildings. The most significant feature is the inclusion of the effects of gravity columns, which is given a full treatment in this article due to its significance to seismic design practice.

A brief description of the test building and testing methodology are presented first to show how the structure was constructed and tested at UCSD. Next, the description of the improved analytical model used to characterize the response of the test building using measured properties is presented, with emphasis on overcoming the limitations of the original model. The analytical results, including envelopes of design forces, floor level displacements, and inter-story drift ratios as well as time-histories of the base moment, top floor displacement, and top floor acceleration of the structure, are then presented and compared with the experimental values. Finally, based on the comparison of results, lessons learned from participation in the blind prediction contest and recommendations to improve seismic modeling of buildings consisting of structural walls and gravity columns are presented.

2. Test Building and Test Methodology

Figures 1a and 1b show, respectively, the floor plan and elevation of the test building which consisted of a 4.88 m long cast-in-place (CIP) flange wall, a 3.66 m long CIP web wall, and a C-shaped precast, segmental pier with unbonded post-tensioning. The web wall primarily provided the lateral force resistance in the earthquake loading direction, while the flange wall and precast pier primarily provided stability in the transverse direction and torsional resistance for the test building. In addition, four pin-ended Dywidag prestressing bars, 44.5 mm in diameter for the first story and 25.4 mm in diameter for the second story and above, were used as columns within each story. The Dywidag bars were grouted inside 101.6 mm diameter, 8.6 mm thick steel pipes to prevent them from experiencing buckling. Due to the pin-ended connections, these columns were assumed in design to act as gravity columns and not to contribute to lateral

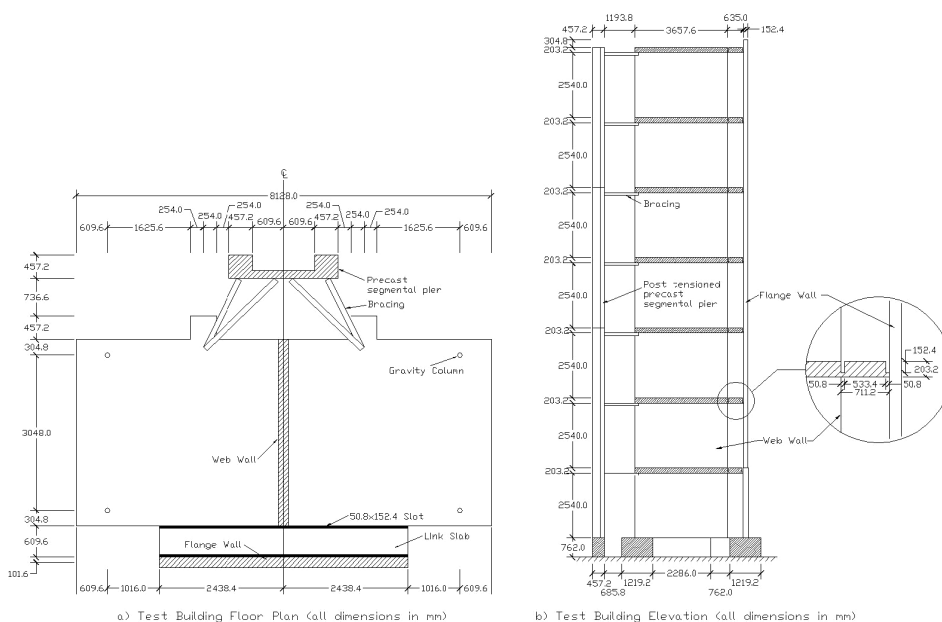


FIGURE 1 Floor plan and elevation of the test building [after NEES7Story, 2006].

force resistance. The floor at each level was 3.66 m wide, 8.13 m long, and 203.2 mm thick reinforced concrete slab, and was supported by the web wall and four steel columns.

Both the flange and web walls had fixed connections to the shake table, while the precast pier connection to the shake table was designed to act as a pin in the loading direction while providing large moment resistance in the orthogonal direction. This was achieved by aligning the post-tensioning tie-downs to the shake table in the direction orthogonal to the direction of the shaking such that it led to relatively small moment resistance in the loading direction. Discussions with researchers at UCSD confirmed that the longitudinal mild steel reinforcement in the pier was not extended into the foundation and that pier was free to rock at the base. The flange wall and the precast pier were designed to have pin connections to the floor slab. Figure 1b includes a magnification of the link slab connecting the main floor slab and web wall to the flange wall. The link slab incorporated two 152.4 mm deep by 50.8 mm wide slots in the slab near the flange wall to accomplish the pin connection to the main floor slab. The pin connection between the pier and the floor slab was accomplished by using steel angles bolted to the floor slab and precast pier. The bolted connections and the limited moment capacity of the angles prevented the transfer of moment from the main floor slab to the pier.

The shake table testing of the building included several input motions, which were: one low amplitude white noise, three low intensity earthquakes, and one high intensity earthquake. The low intensity earthquake records chosen were the longitudinal (EQ1) and transverse (EQ2) components from the 1971 San Fernando earthquake recorded at site, *vnuy*, and the longitudinal component from the 1994 Northridge earthquake at site, *whox* (EQ3). The high intensity record was the 360° component taken from *Sylmar Olive View Med* (EQ4) that was recorded in the 1994 Northridge earthquake located near the epicenter of the earthquake [NEES7Story, 2006]. The strongest 30 s of ground motions EQ1, EQ2, EQ3, and EQ4 are shown in Fig. 2, while the response spectra of these

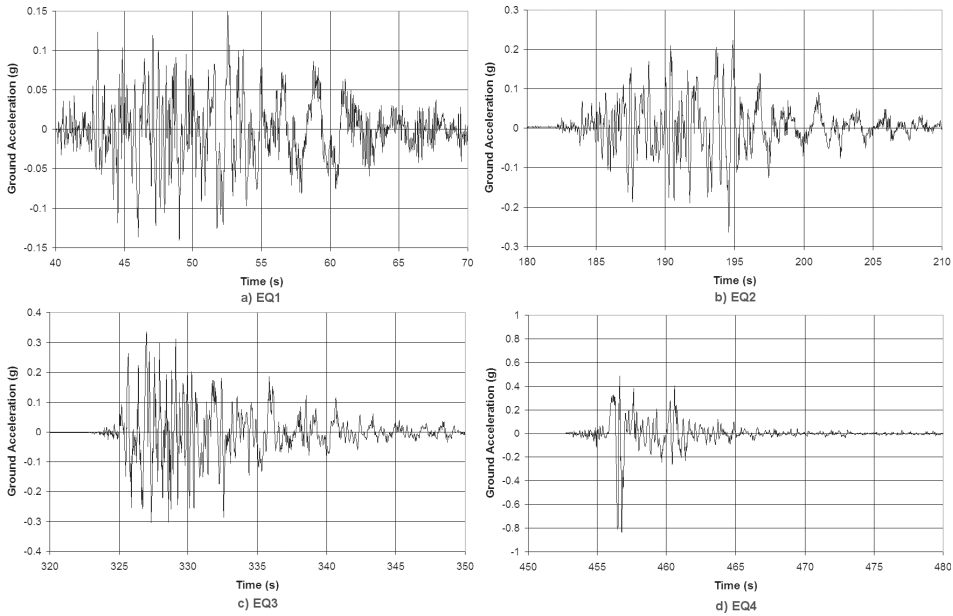


FIGURE 2 Earthquake input motions used for the shake table test.

motions corresponding to 5% viscous damping are shown in Fig. 3. The input ground motions for the blind prediction were given at both 50 and 240 Hz; the 50 Hz motions were selected for the dynamic analyses reported in this article. The low-intensity input motions were expected to cause limited damage to the test building while the high-intensity earthquake was anticipated to cause significant damage. In all cases, the plastic hinge and the associated damage was expected to concentrate in the first floor level of the test building.

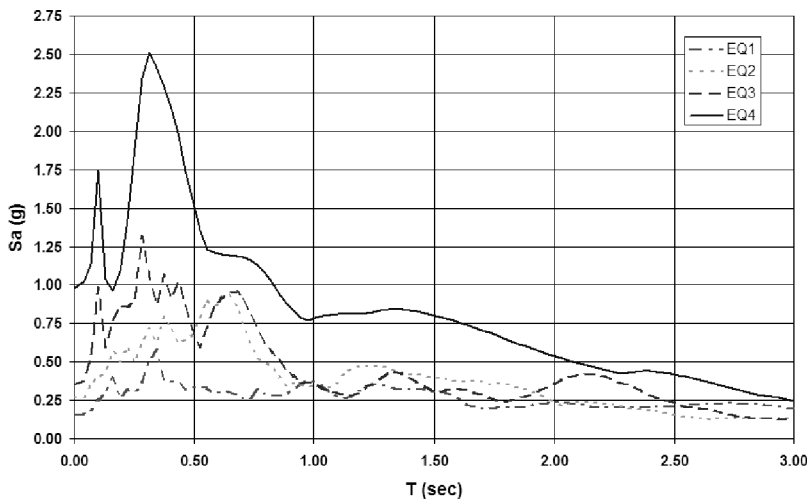


FIGURE 3 Earthquake input motions response spectra with 5% damping.

3. Analytical Model and Key Features

The original model used for the blind prediction contest was a simple centerline model that included the web wall, flange wall, and post-tensioned segmental pier. As previously stated, this model was generally satisfactory in predicting the displacements and accelerations, but not overturning moments. The concept and relevant details of the improved model, together with discussion of critical issues that eliminated the deficiencies of the original model are presented below.

3.1. Overview

As noted, both the original and improved models of the test building were created to balance the need for accuracy with the desire for a relatively simple model that would run quickly and could be built based on the geometry and measured material properties. Because the accelerations were only applied in one direction, a two-dimensional model parallel to the web wall was preferred. OpenSees [Mazzoni *et al.*, 2004] was selected as the analysis software because of its use in an ongoing PreNEESR project that focuses on concrete wall buildings [Sritharan *et al.*, 2005]. As part of this project, the capabilities of OpenSees for analyzing walls have been studied and new features have been added [e.g., Zhao and Sritharan, 2007].

The seismic mass of the structure was lumped at the floor levels to simplify the model and expedite the analysis. The mass corresponding to each floor was calculated by determining the mass of the floor slab and one half-story height of the flange wall, web wall, pier, and gravity columns above and below the floor, and concentrated at the node located at the floor level. The weight of the structure was also applied as point loads on the nodes at each floor level to account for the gravity effects. Table 1 summarizes the point loads and masses applied to the model.

The number of elements and nodes in the improved analytical model maintains the simplicity and efficiency of the original model. A diagram delineating the improved OpenSees model is shown in Fig. 4, which had a total of 83 nodes and 81 elements including 56 beam-column elements, 22 truss elements, and 3 zero-length interface elements. In comparison, the models used by other participants had as many as 3,143 elements and 3,360 nodes [Restrepo, 2006].

TABLE 1 Nodal gravity forces and masses

Location	Nodal force (kN)	Mass (kN*s ² /m)
1 st Floor Web Wall	46.26	4.72
1 st Floor Flange Wall	61.70	6.29
1 st Floor Pier	36.14	3.68
2 nd –6 th Floor Web Walls	105.87	10.79
2 nd –6 th Floor Flange Walls	60.50	6.16
2 nd –6 th Floor Piers	36.14	3.68
7 th Floor Web Wall	71.17	7.25
7 th Floor Flange Wall	19.57	1.99
7 th Floor Pier	36.14	3.68

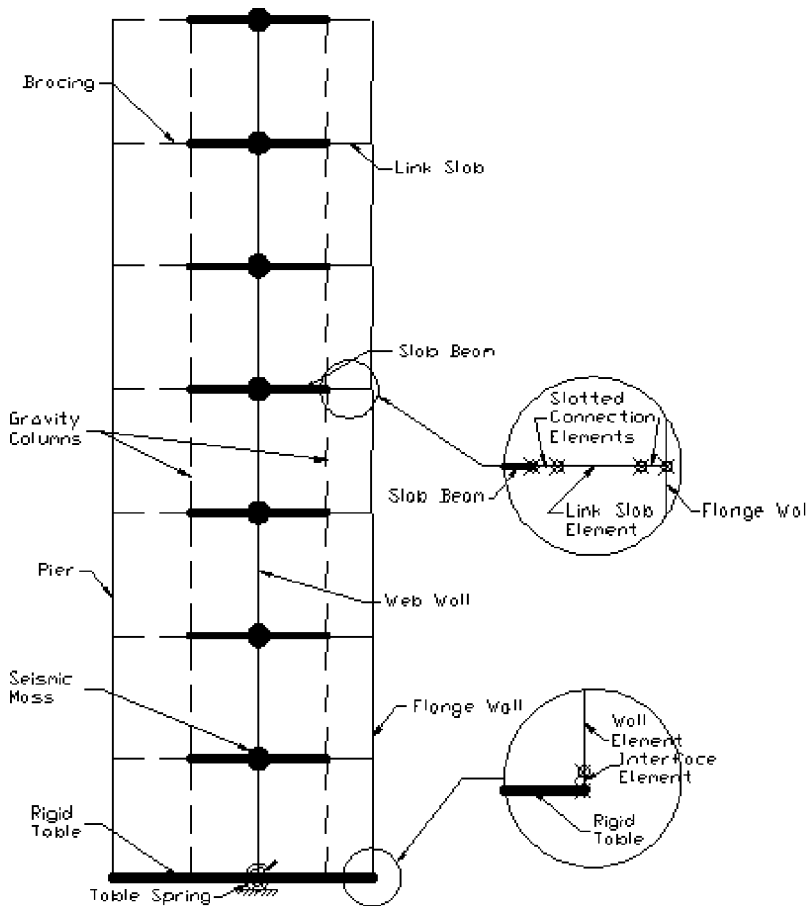


FIGURE 4 Schematic of the improved OpenSees model diagram of the test building.

3.2. Lateral Force Resisting System

Based on the previous work done in modeling the response of structural walls to cyclic displacements by the writers, the flange and web walls of the test building were modeled using fiber-based beam-column elements. Due to difficulties in obtaining compatible forces and deformations for the force-based beam-column elements modeling the flange and web walls in the dynamic analysis, displacement-based beam-column elements were chosen. However, the first-story web and flange walls were modeled using the force-based beam-column elements because they are considered to be a better choice for modeling the plastic hinge regions [Neuenhofer and Filippou, 1997]. The beam-column elements were assigned fiber sections that discretely modeled the reinforcement as well as confined and unconfined concrete regions. The first floor web wall section was discretized using 100 confined concrete fibers and 302 unconfined concrete fibers, while the first-floor flange wall section was discretized with 20 confined concrete and 456 unconfined concrete fibers. The sections for the upper-level flange wall used 60 unconfined concrete fibers to discretize the wall, while the upper-level web wall section used 72 unconfined concrete fibers. A single beam-column element with five integration points along the element length was used to represent each wall within each story. The choice of

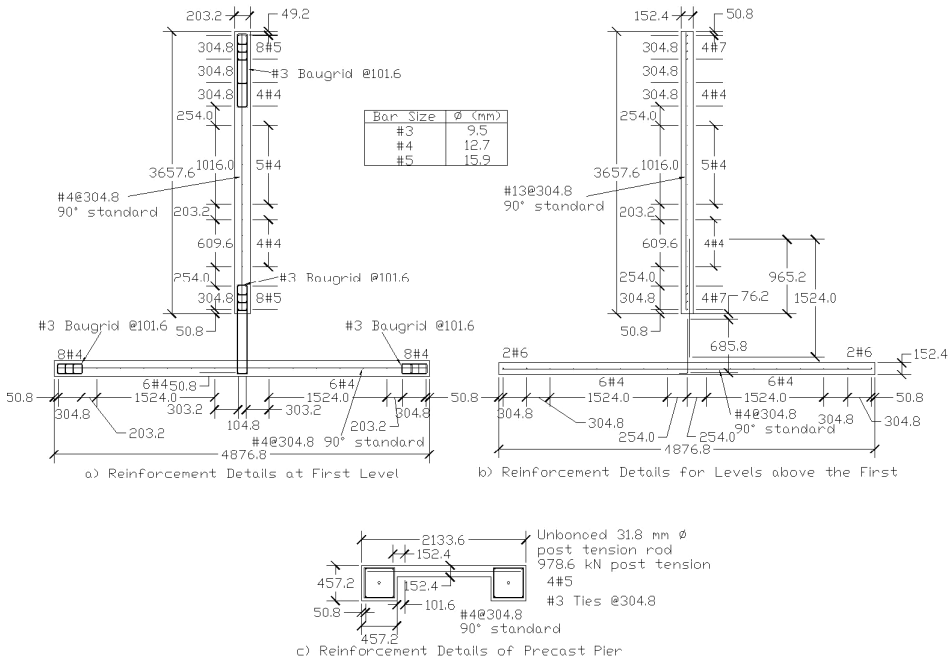


FIGURE 5 Wall and pier reinforcement details [after NEES7Story, 2006].

using five integration points for the beam-column elements representing the walls at each floor level was based on the experience of the OpenSees community, and that of the writers' work on simulating the response of concrete walls.

The fibers representing the longitudinal reinforcement in various elements were located according to the as-built drawings shown in Figs. 5a and 5b, which depict the dimensions and reinforcement details of the flange and web walls at the first floor and for floors two through seven, respectively. The properties of the confined concrete were calculated using the transverse reinforcement details and the confined concrete model proposed by Mander *et al.* [1988], and were assigned to the corresponding fibers in the wall cross-sections at the first story of the building model. The upper stories had no confinement reinforcement and thus the concrete was modeled using unconfined concrete fibers. Material models "Steel02" and "Concrete03" available in OpenSees were used to model the reinforcing steel and concrete behavior. The properties of the unconfined concrete and steel reinforcement material models were chosen to closely match the experimental stress-strain behavior established for these materials. Figures 6a and 6b show the measured and modeled monotonic stress-strain curves of the unconfined concrete in the first story walls and the #4 ($d_b = 12.7$ mm, where d_b is the bar diameter) longitudinal bars used in the flange and web walls, respectively. It can be seen that the chosen concrete model adequately captures the unconfined concrete behavior. The behavior of the reinforcing steel was accurately modeled up to a strain of about 0.06 and significant discrepancies between the measured and modeled behaviors were expected at larger strains. To account for the low-cycle fatigue behavior, the fracture strain for the longitudinal reinforcement was taken as 0.06 and thus the longitudinal steel reinforcement strains were limited to 0.06 during the analysis. The tension capacity of concrete was modeled using a peak tensile strength of $0.59\sqrt{f'_c}$ with nonlinear post-peak softening

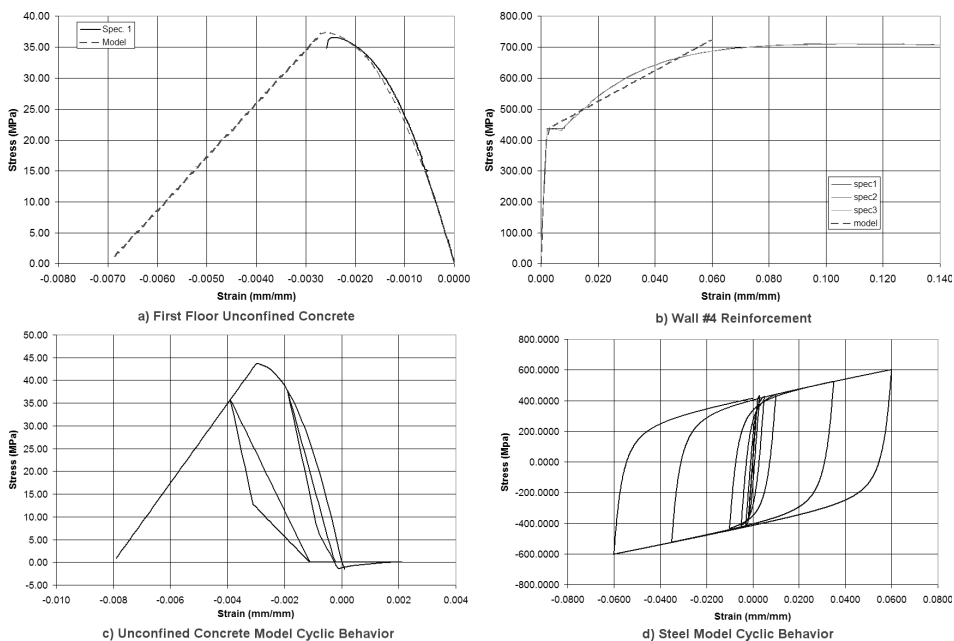


FIGURE 6 Material model comparisons.

following the University of Houston model proposed by Hsu [1993], where f'_c is in MPa. Figures 6c and 6d show the cyclic response characteristics of the steel and concrete material models, while the parameters used for the concrete and reinforcement material models in the analysis are given in Tables 2 and 3, respectively.

The strain penetration effects resulting from anchoring of the wall longitudinal reinforcing bars into the foundation block were included in the model using a zero-length section element with the same cross-section as the wall element above it. However,

TABLE 2 Concrete material properties as defined in OpenSees

Location	Peak compressive stress (MPa)	Peak compressive strain (mm/mm)	Ultimate compressive stress (MPa)	Ultimate compressive strain (mm/mm)	Peak tension stress (MPa)	Peak tension strain (mm/mm)
1 st Level Walls Unconfined	37.4*	0.002664*	0.0	0.007	3.8	0.000135
2 nd –6 th Level Walls	39.3*	0.002307*	0.0	0.007	3.9	0.000144
Precast Segmental Pier	38.8*	0.002375*	0.0	0.007	3.9	0.000119
Slab Beams & Link Slab	37.4*	0.002664*	0.0	0.007	3.8	0.000136

* Based on the average response of tested concrete cylinders.

TABLE 3 Steel material properties as defined in OpenSees

Size & location	Yield stress (MPa)	Young's modulus (MPa)	Strain hardening ratio
#4 - Flange and Web Walls	434.4*	199,948*	0.025
#5 - Flange and Web Walls	434.4*	199,948*	0.0225
#6 - Flange and Web Walls	475.7*	199,948*	0.025
#7 - Flange and Web Walls	461.9*	199,948*	0.025
#4 - Precast Pier	461.9*	199,948*	0.025
#5 - Precast Pier	489.5*	199,948*	0.025
Pier Bracing	248.2	199,948	0.01
Gravity Columns	879.1	199,948	0.01

* Based on the average response of tested reinforcement bars.

the steel material model in this element was replaced with the strain penetration model developed by Zhao and Sritharan [2007], which describes the total bar slip due to strain penetration as a function of stress in the bar. This accounted for the additional flexibility resulting from the wall end rotation due to penetration of strain along the longitudinal reinforcement into the foundation block. The bottom node on the interface element was fixed for all degrees-of-freedom while the top node was only restrained against lateral translation. The bottom ends of the beam-column elements modeling the first-story flange and web walls of the building were connected to the top nodes of the interface elements.

The unbonded post-tensioned pier was also modeled using displacement beam-column elements. A fiber section was used to represent the pier cross-section shown in Fig. 5c. The section was defined using 40 unconfined concrete fibers; the material properties used for the pier concrete and reinforcement are included in Tables 2 and 3, respectively. Similar to the flange and web walls, a single beam-column element with five integration points along the element was used to represent the pier within each story. Anticipating primarily an elastic response, the unbonded post-tensioning rods in the pier were modeled using a single truss element that was given an elastic perfectly plastic material behavior and an initial strain to simulate the effect of prestress. The truss element shared the nodes at the top and bottom of the beam-column element modeling precast pier without any additional constraints along the height of the pier. Since the pier base moment resistance was relatively small and had limited impact on the overall response, this approach was deemed appropriate. As previously noted, the base of the pier was not rigidly connected to its foundation, but it allowed a small moment resistance to be generated at this location by developing compression force at the base of pier and tension force in the post-tensioning rods. The braces connecting the pier to the floor slab (see Fig. 1a) were modeled using truss elements and the Steel02 material model. The truss elements connected the nodes at floor levels on the post-tensioned pier to the nodes at the end of the floor slab elements.

3.3. Floor Slabs and Gravity Columns

As discussed, the gravity columns were very important to the overall structural response, but were ignored in the original model. Consistent with the design assumptions, most

participants in the blind prediction did not model the floor slab and columns because the specially detailed pinned connections at the column ends were intended to remove them from providing the lateral load resistance. However, the influence of the gravity columns and floor slab on the overall force-displacement response of the test building was evident during testing, and was confirmed by Panagioutou and Restrepo [2006] using a pushover analysis of the building. The primary reason for this influence was that the columns developed significant axial strains during testing due to their interactions with the floor slab. Consequently, the columns closer to the compression side of the web wall were subjected to compression forces and those near the tension side of the web wall were subjected to tensile forces. This enabled a large moment couple to be developed due to the distance of 3.05 m between the compression and tension columns, effectively contributing up to 24% to the lateral force resistance of the test building. The interaction between the floor slabs and gravity columns were dictated by the flexural stiffness of the floors, fixed connection between the slab and walls, and axial constraints imposed to the floor slabs by the gravity columns. Therefore, it was expected that the extent of the flexural cracking of the concrete floor slab occurring perpendicular to the direction from the compression region of the web wall to the tension columns and tension region of the web wall to the compression columns to have influenced the amount of force developed in the gravity columns. Figure 7 shows a part of the 3D ANSYS [Swanson Analysis Systems, 1992] model created to understand the interaction between the floor slab and gravity columns. The ANSYS model included the web wall, floor slab, and four gravity columns per floor for the seven floors in the building slice. The floor slab and web wall were modeled using the concrete element Solid65, but the flange wall was not modeled. This element is an eight node brick element that incorporated tension cracking and compression crushing of the concrete material, but the latter capability of the model was turned off because crushing of concrete can prematurely occur in an ANSYS analysis as reported by Barbosa and Ribeiro [1998]. The effect of the confined concrete was modeled by modifying the uniaxial behavior defined for the material in the boundary elements of the web wall using the confined concrete model of Mander *et al.* [1988]. The longitudinal and transverse reinforcement in the Solid65 element is smeared across the element area and defined with orientation relative to the global coordinate system and a uniaxial material model describing its stress-strain characteristics. The nodes along the top of the wall in the model were constrained to displace equally in the direction parallel to the length of the web wall. The behavior of this 3D model was studied by imposing monotonic displacement pattern that followed the first mode response of the test building.

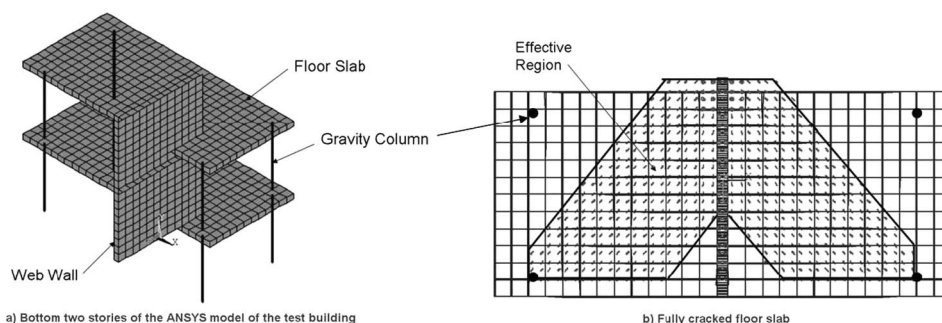


FIGURE 7 The ANSYS model used to understand the 3D effects of the floor slab.

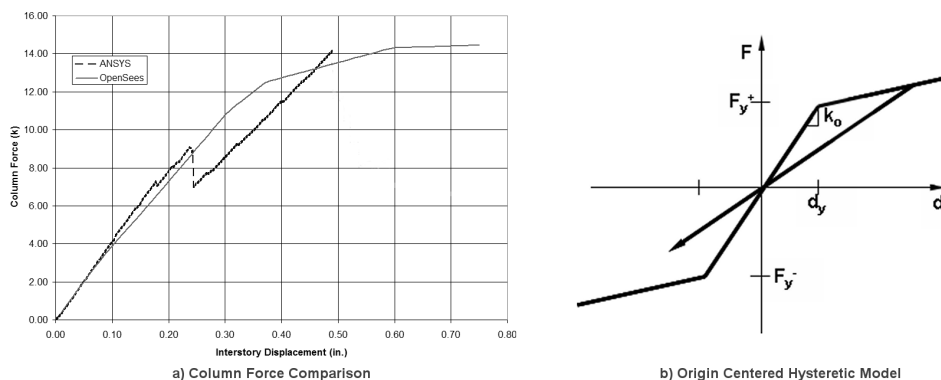


FIGURE 8 Calibration of axial force induced in columns vs. inter-story displacement and the model chosen for the cyclic behavior.

The 3D slab effect was introduced into the 2D OpenSees model using a beam-column element at each floor level. A bilinear moment-curvature envelope was selected to define the section behavior of this element. The initial slope of the moment-curvature relation is based on the uncracked slab properties with the flexural stiffness of 1,130 and 3,390 MN-m-rad for the positive and negative moments, respectively. The two different stiffness values are due to the different reinforcement mats in the top and bottom of the slab. The moment at the transition between the two linear portions was defined by the flexural cracking moment occurring over an effective width of the slab. This moment was estimated to be 152.5 kN-m, based on an effective slab width of 11.5 times the slab thickness (or 2.33 m) that was determined from the ANSYS analysis results (see Fig. 6b). A post cracking stiffness ratio of 20% that was determined using the nominal strength and the corresponding curvature of the slab section over the effective width defined the second slope. This approach for modeling the 3D effects of the slab-to-gravity column interaction in the 2D OpenSees model was validated by comparing the axial force induced in the columns vs. inter-story displacement with that obtained from the ANSYS model. Figure 8a depicts this response at the first story level and confirms that the 3D effects of the slab-column interaction was satisfactorily addressed in the 2D model, while Fig. 7b shows the origin centered hysteretic model used for the moment-curvature behavior of the section of this beam-column element.

The gravity columns were modeled using truss elements with the appropriate cross-sectional area to simulate the axial constraints provided by the Dywidag bars. Since the OpenSees model was only 2D, the area of the two columns on each end of the web wall were modeled with a single truss element with twice the area of a single column. Small rigid links were used to model the thickness of the floor slab to accurately simulate the clear length of the gravity columns.

3.4. Link Slab Connection

Similar to the gravity columns, the effects of the link slabs were typically overlooked by the participants in the blind prediction contest. The link slab shown in Figs. 1a and 1b refers to the regions where notches were cut in the portion of floor slab connecting the flange and web walls. The intent of this detail was to minimize the moment resistance at the flange wall-to-slab interface while allowing the transfer of in-plane inertia forces.

Despite minimizing the moment, a significant shear along the length of the notch was possible, which, in turn, increased the axial load in the web wall. Panagioutou and Restrepo [2006] also observed this stiffening effect in their pushover model and showed that it almost doubled the axial load on the web wall when yielding of the horizontal notch reinforcement occurred as observed in the test.

In the original model, the effect of the notches was included by constraining the lateral displacements of the flange and web wall, while the rotational DOFs for the flange and web wall nodes were not constrained. Other participants in the contest used similar approaches by using either constraint equations or truss elements to model the effect of the link slab; however, neither approach captures the axial stiffening of the web wall and associated increase in the lateral force resistance adequately. In the improved model, the link slab was modeled using three beam-column elements with fiber sections. Two beam-column elements were used to model each of the reduced sections of the slot, and the third beam-column element modeled the slab between the slots. The cross-sections for both the slab and slot regions were modeled using fibers representing the unconfined concrete and longitudinal reinforcement. This approach allowed yielding of the slab reinforcement along the notch, imposing the appropriate amount of additional axial load on the web wall. The additional axial load increased the resistance of the web wall by approximately 16%.

The beam-columns elements modeling the notch did not include the effects of shear deformation. It is not clear if the notch regions sustained significant shear deformation. However, the UCSD researchers did not provide any specific information about this issue in their discussions of the behavior of the link slab.

3.5. Table and Foundation Flexibility

The connection between the test building and the shake table was modeled in the boundary conditions for the wall and pier elements. However, the shake table and foundation as a whole experienced some rotation and the building's response was influenced by the rotational stiffness of the table. The table flexibility was neglected in the original model. As shown in Fig. 4, a zero-length elastic rotational spring was used to account for this additional flexibility in the improved model; rigid beams were used to link the rotational spring to the bases of the web and flange walls, gravity columns, and precast pier. Table 4 lists the rotational stiffness of the table and foundation measured in each direction by the UCSD researchers for each of the ground motions. As indicated in this table, the average rotational stiffness obtained from the stiffness reported for the two directions during testing to EQ2, EQ3, and EQ4 defined the behavior of the rotational spring in the improved analytical model. The rotational stiffness reported for EQ1 was relatively high compared to the values for the other events and thus was not included when finding the average value. This approximation was preferred since the effects of all earthquakes were examined in one

TABLE 4 Base spring rotational stiffness

	Rotational spring stiffness due to combined flexibility of table and foundation *10 ⁻⁷ (kips-ft/rad)				
	EQ1	EQ2	EQ3	EQ4	Model
Direction 1	1.326	0.883	0.711	0.711	0.7904
Direction 2	1.378	0.888	0.684	0.746	0.7904

analysis and the expected error in displacement due to underestimating the table stiffness for EQ1 was found to be less than 5%. With this average value representing the rotational stiffness, one node of the rotational spring was fully fixed against deformation while the other node was allowed to rotate parallel to the web wall.

3.6. Influence of Shear Deformation

Experimental research has shown that shear deformation can contribute significantly to the lateral displacement, especially at the lower floor levels, even in slender, flexure-dominated walls [e.g., Thomsen and Wallace, 1995]. The effects of shear deformation need to be included to better simulate the lateral displacement, especially at the lower floor levels. The fiber sections used for the wall in the original model did not include any shear effects in the section formulation, requiring the shear response to be handled separately.

Some of the other participants did not have to separately handle the shear deformation because the modeling approach they used included the effects of shear within their chosen elements. However, OpenSees did not have an option for including shear in the selected element definition and the fiber sections used in the analysis sums the uniaxial response of the fibers to determine the axial and moment resistance of the section. Because the fibers have zero resistance to transverse loads, the shear deformation cannot be determined at the section level. In the original model, an estimate of the additional lateral displacement due to shear deformation was added during post-processing of the results. In the improved model, the shear force-deformation response was added to the beam-column elements modeling the web wall during the analysis. The shear deformation of the flange wall was, however, neglected since its resistance was relatively small and the short dimension of the wall section was parallel to the direction of shear force. Aggregating the shear response onto the flexural response does not cause the axial strains experienced by the fibers due to curvature of the wall to change, neglecting the possible flexure-shear interaction.

The lateral force vs. shear deformation hysteretic response of the web wall was modeled using a uniaxial material model. Figure 9 shows the “pinching4” material model available in OpenSees that was used for this purpose at the first floor level. A

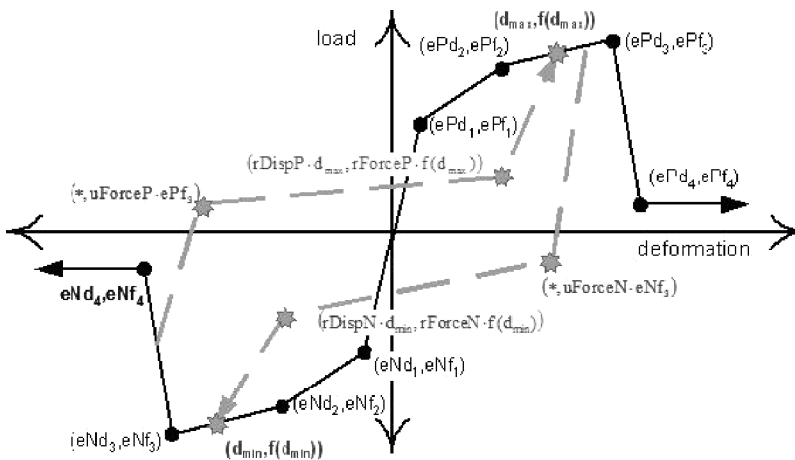


FIGURE 9 Pinching4 material model used to account for the shear deformation contribution [Mazzoni *et al.*, 2004].

minimum of three points with an optional fourth point are needed to define the response envelope for this model. Because the measured shear deformation of the web wall was not available, only three points were defined for the pinching model as follows: (1) point 1 was defined using the lateral force corresponding to the first flexural cracking of the web wall (111.2 kN) and the uncracked shear stiffness; (2) point 2 was defined using the lateral force that was expected to cause flexural yielding of the longitudinal reinforcement (311.4 kN) and effective shear stiffness; and (3) point 3 was defined using the ultimate lateral force resistance (467.1 kN) and post-yield shear stiffness. The uncracked shear stiffness was obtained following the recommendation of Park and Paulay [1975] for an uncracked rectangular beam. The effective shear stiffness to the uncracked shear stiffness was taken as the same ratio as the flexural stiffness at yield to the gross flexural stiffness; this ratio was determined to be 20% of the uncracked stiffness. This choice to relate the cracked shear stiffness to the cracked flexural stiffness was based on observations of the behavior of RW2 and TW2 tested by Thomsen and Wallace [1993], RWN and NTW1 tested by Brueggen *et al.* [2007], and the rectangular walls tested by Oesterle *et al.* [1979]. Furthermore, research by Massone and Wallace [2004] showed that when inelastic flexural action occurs, inelastic shear action also begins because of coupling of the two responses. In order to simulate this coupling, the lateral force at yield was used to define the point when the tangent stiffness changes from the effective shear stiffness to the post-yield shear stiffness. The post-yield stiffness was defined based on the observed shear force versus deformation responses of NTW1 and RWN from the PreNEESR wall tests [Brueggen *et al.*, 2007] and RW2 and TW2 tested by Thomsen and Wallace [1995]. Based on those data sets, the post-yield shear stiffness was approximated to 1.0% of the effective shear stiffness. Shear stiffness for the second floor and above was modeled using an elastic material model with stiffness equal to 35% of the uncracked shear stiffness to reflect the cracking of the wall.

3.7. Viscous Damping

OpenSees includes Rayleigh damping as an option to capture the effects of the viscous damping during dynamic analysis. In a nonlinear system, the stiffness matrix used for calculating the damping matrix can have a significant impact on the results of the analysis. In the original model, Rayleigh damping was used in conjunction with the current stiffness matrix, allowing damping to decay as the damage accumulated. The coefficients needed to define the Rayleigh damping were obtained assuming 5% viscous damping for the first and third modes that were found from cracked section properties.

Priestley and Grant [2004] recommended that tangent stiffness proportional damping be used for nonlinear analysis because Rayleigh damping heavily weights the mass matrix, leading to an almost constant damping matrix during the nonlinear response of the structure regardless of the degradation that occurred to the stiffness of the structure. Furthermore, observations by Moaveni *et al.* [2006] of the test building indicated approximately 3% damping on the first longitudinal mode when testing to white noise. However, Panagioutou and Restrepo [2006] used only 0.3% damping for the first longitudinal mode for accurate simulation of the test building's response to earthquake input motions. Such low damping may have been due to excluding the non structural elements in the test structure and limiting flexural cracking largely to the lower portion of the building due to the use of reduced longitudinal reinforcement. Consequently, in the improved model stiffness proportional viscous damping corresponded to 0.5% damping on the uncracked first mode period and 0.8% damping on the uncracked third mode period was used. This resulted in 0.02 and 0.5% viscous damping, respectively, on the cracked first and third

mode responses of the building. Since the damping was determined from the tangent stiffness matrix as recommended by Priestley and Grant, viscous damping was further reduced during response in the post-yield region.

3.8. Dynamic Analysis

The input accelerations shown in Fig. 2 were applied to the base of the building model in the direction parallel to the web wall. Using the Newmark's constant average acceleration method for the integrator, the analysis was conducted at a time increment of 0.02 s to limit the amount of output that must be post-processed. However, when the analysis failed to converge, 10 substeps were carried out at 0.002 s to find a solution, and then the time step was increased back to 0.02 s.

In order to account for the effects of accumulated structural damage on the response of the test building, all input motions were concatenated. Six seconds of zero ground acceleration was added between the earthquake records to allow the structure to come to rest prior to being subjected to the next base input motion. The low accelerations at the end of the ground motions combined with the 6 s of padding were adequate for the structure to return to rest. The total applied ground motion record to the test building was slightly more than 522 s long from start to finish. The entire analysis took approximately 45 min to run on a 2.0 GHz Pentium IV based-computer with 1 GB of RAM running Windows XP.

4. Comparison of Results

The capabilities of the improved model can be seen best by comparing key time-history responses with the measured data provided for the test building [NEES7Story, 2006]. For this purpose, the top-floor displacement, base moment, and top-floor acceleration are used. This is followed by comparison of envelope responses for variables that are of interest from a design viewpoint.

4.1. Time-History Responses

4.1.1. Top-Floor Displacement. The top-floor displacement time-history is shown in Fig. 10 with a, b, c, and d representing, respectively, the response during the most intense 30 s of EQ1, EQ2, EQ3, and EQ4. The figures show that the period of the test building was well captured by the analysis model for all earthquake intensities, except around 12–15 s into the EQ4 motion. Table 5 shows the period of the structure at various stages of loading. The analytical model simulated the period of the structure within 0.1 s. Additionally, all the significant peak displacements recorded during EQ1, EQ2, and EQ4 were generally well simulated, and were within 5% of the measured values. The peaks on EQ3 were under predicted by as much as 25%.

The cause of the discrepancy for the EQ3 event was extensively studied, because similar discrepancies were observed in the predictions by other participants (e.g., Kelly, 2007). The fact that EQ2 and EQ3 were comparable to each other in earthquake intensity was the primary cause for large discrepancies in the response of EQ3 and consequently the unloading and reloading behaviors of the material models rather than their envelopes had a large influence on the analytical response of EQ3. Typically, the response envelopes of materials are more accurately characterized than their reloading and unloading action. This hypothesis was confirmed by scaling

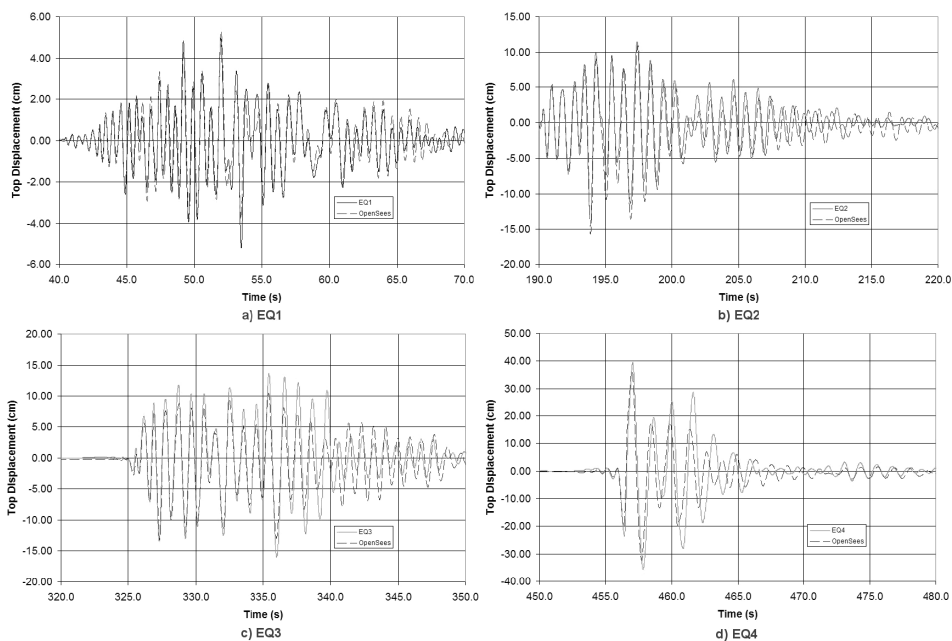


FIGURE 10 Comparison of measured and simulated displacement time-histories.

TABLE 5 Comparison of measured and calculated structure fundamental period

	Measured period (s)	Calculated period (s)
Before Testing	0.526	0.519
Following EQ1	0.613	0.620
Following EQ2	0.826	0.873
Following EQ3	0.893	0.90
Following EQ4	0.980	0.974

the accelerations of EQ2 by 0.6 without altering the other events and rerunning the analysis. This modification significantly improved the EQ3 response of the test building, bringing the peak displacements for this event to within 5% of the measured values. The concrete material model used for the analysis here used very simple unloading and reloading behavior, as shown in Fig. 6c. The poor simulation of EQ3 is, therefore, expected to be improved by using an improved constitutive model for concrete with more accurate representation for the unloading and reloading paths. Furthermore, the pinching4 model may not be adequately simulating the shear deformation of the web wall; however, without the measured data for the shear deformation, the accuracy of the shear behavior cannot be evaluated. The simple unloading and reloading behavior of the pinching4 model was also expected to have influenced the response of the test building to EQ3.

4.1.2. Base Overturning Moment. The base moment was determined by summing the moments at the base of the web and flange walls, and the couple generated by the gravity columns that had about 10–24% contribution to the base overturning moment. Time history comparison for the base moment is shown in Fig. 11, in which many of the characteristics observed for the top-floor displacement time-history are also seen in the base moment plot comparison. Again, it is noted that the period of the structure was well captured, showing that the analysis adequately captured the damage and subsequent softening of the structural stiffness. The peak values were generally well captured and are within 10–15% of the measured values for EQ1, EQ2, and EQ4. As expected, the response of EQ3 was not as well simulated giving results within 25% of the measured values due to the aforementioned reasons.

4.1.3. Top-Floor Acceleration. The top-floor acceleration time histories for all ground motions are shown in Fig. 12. The acceleration time history shows the expected response considering the under prediction of the lateral displacement. Despite capturing the period of the structure accurately, the peak floor accelerations are typically over predicted by the analysis by approximately 10–20% when compared with the responses measured during the test.

The simulation of the top-floor acceleration was generally considered satisfactory given the large time step used for the input excitations used for the analysis and analysis time step. Simulation of the accelerations in a dynamic analysis can be sensitive to the time step used in the analysis and it typically requires a small time step to obtain accurate acceleration responses. The large time step used in the analysis allows a good simulation of the floor level accelerations without requiring an extensive amount of computational time needed to use a small time step and post-process the corresponding analysis output.

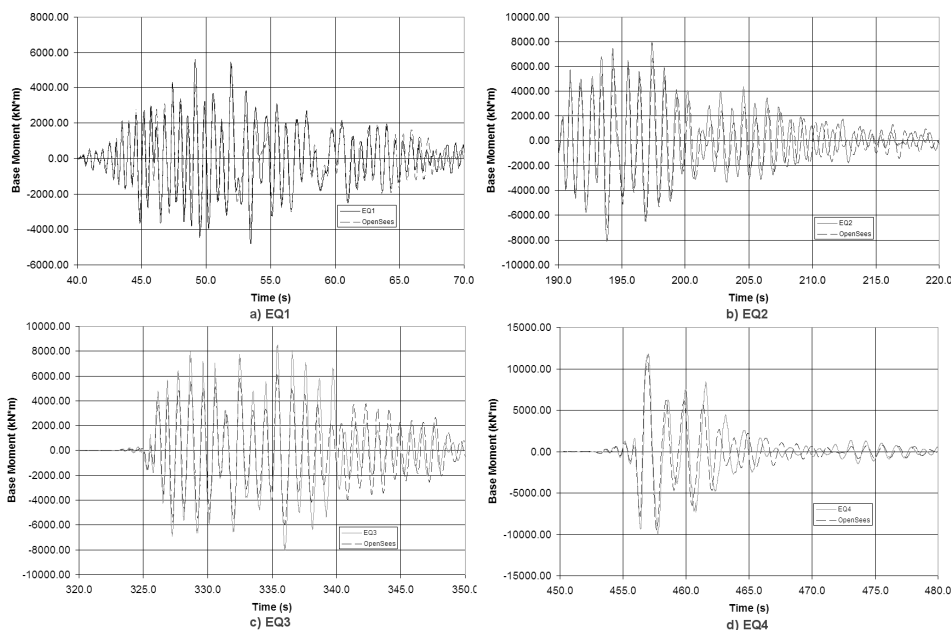


FIGURE 11 Comparison of measured and simulated base moment time-histories.

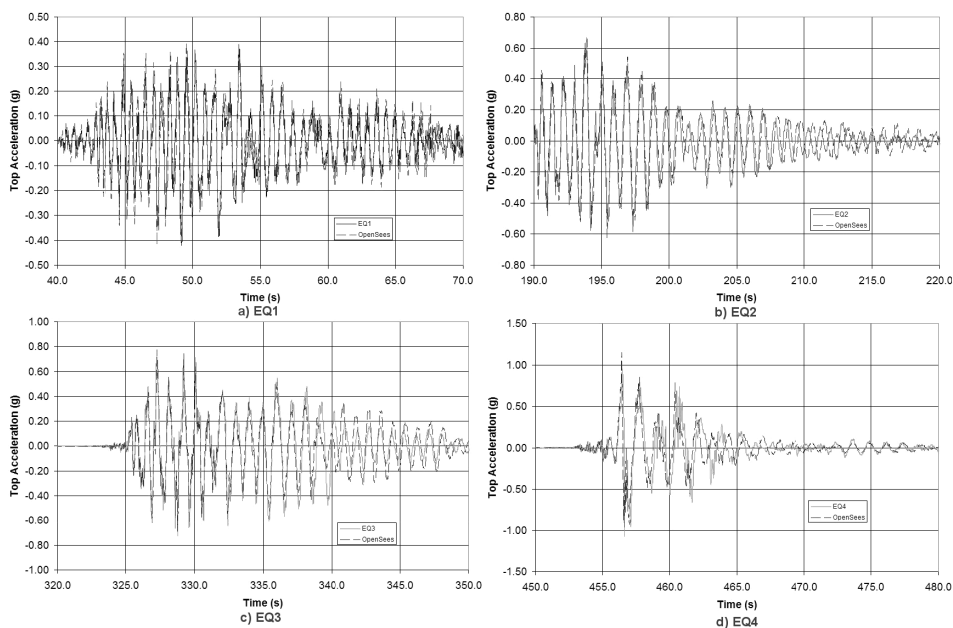


FIGURE 12 Comparison of measured and simulated acceleration time-histories.

4.2. Envelope Responses

The envelope responses of the test building model along with their experimental values are shown in Figs. 13 with a, b, c, and d representing the lateral displacement, inter-story drift, overturning moment, and story shear, respectively. The comparisons of the envelopes are discussed below in recognition of their influence on design.

4.2.1. Lateral Displacement. The floor-level lateral displacements shown in Fig. 13a are generally well simulated, with the exception of EQ3. The displacements of EQ3 were under predicted by about 17%. For the rest of the ground motions, the predicted lateral floor displacements were within 10% of the recorded values during the shake table tests. The top floor displacements were generally better captured than the first floor displacements. This could be due to the influence of the shear deformation, since shear deformation has a larger impact on the lower floor level displacements.

The peak average interstory drift obtained from the top floor displacement divided by the height of the building is used in the design of the structure. Despite designing the building as a flexible structure, the test building did not experience excessive lateral drifts. The maximum average drift ratios were found to be 0.27% for EQ1, 0.81% for EQ2, and 1.88% for EQ4, and the corresponding measured values were 0.27%, 0.76%, and 2.06%, respectively. As expected, a poor comparison was obtained for EQ3 response and the calculated and measured peak average drifts for this event were 0.69% and 0.83%, respectively.

4.2.2. Interstory Drift Ratio. An accurate simulation of the inter-story drift is important to predict the damage to structural as well as non structural elements. The inter-story drift

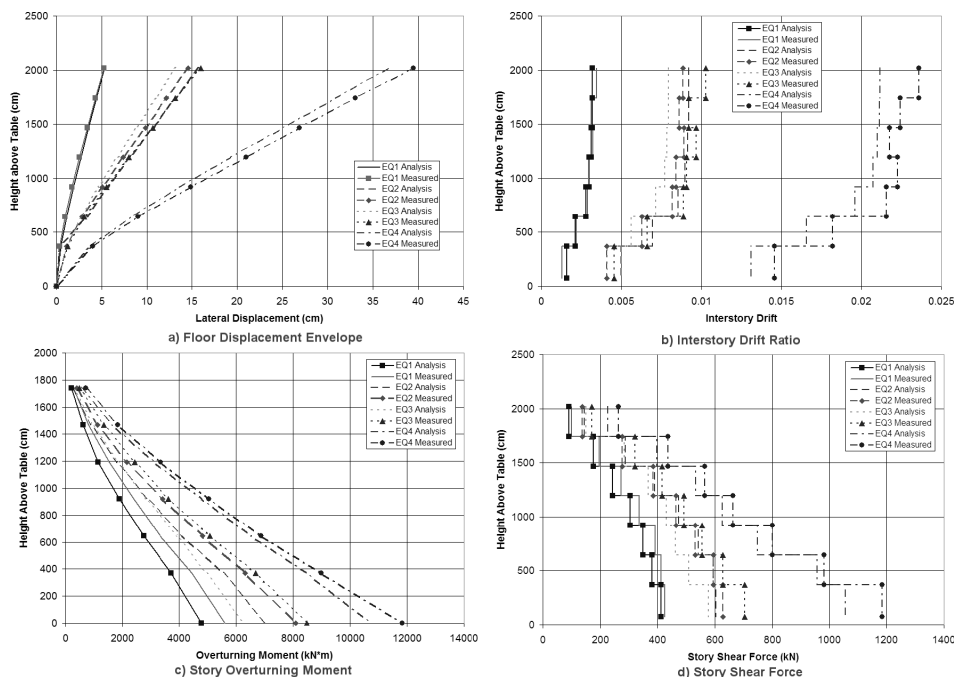


FIGURE 13 Comparison of measured and simulated response envelopes.

ratios, shown in Fig. 13b, were well simulated by the analysis and were within 10% of the experimental values for EQ1, EQ2, and EQ4. The EQ3 inter-story drift was poorly simulated with results being within 20% of the measured values for the reasons previously discussed.

4.2.3. Overturning Moment Envelope. The overturning moments, shown in Fig. 13c, were generally under predicted by the analysis compared to the envelopes established from the measured data. If the results for EQ3 are ignored, then the analytical results were within 5–15% of the recorded values. The results for EQ3 were within 25% of the measured values except for the top two floors, where they were under predicted by 30–40%. The moment generated by the gravity columns contributed 18–24% of the overturning moment resistance for EQ2, EQ3, and EQ4, while approximately 10% for EQ1.

The difference between the measured and calculated overturning moments was expected due to the influence of the higher-mode effects. However, it is noted that the time-history shown in Fig. 11 for the base moment was generally well simulated as a function of time.

4.2.4. Story Shear Forces. The story shear forces, depicted in Fig. 13d, show a similar trend to that observed for the overturning moments. The analysis under predicted the measured responses by approximately 5–15% for EQ1, EQ2, and EQ4; however, EQ3 was under predicted by approximately 25%. As stated before, the analytical response of the test building during EQ3 was controlled by the unloading and reloading behavior of the material models and improvements to the cyclic behavior of the material models would improve the

analytical response of the building to EQ3. Overall, the story shear forces were adequately captured, and an accurate prediction of the shear demand would help ensure that shear failure of the walls would not control the seismic behavior of the building.

5. Summary, Conclusions, and Lessons Learned

A 2D centerline model was created in OpenSees for a full-scale portion of a building that was designed and subjected to shake table tests at UCSD. This model emphasized simplicity and ease of creation based on the geometry and material properties. The original model used beam-column elements to model the flange and web walls, and the post-tensioned pier that was used primarily to provide stability to the test building. The improved model added elements that were ignored in the original model such as the link slab, gravity columns, and a rotational spring to simulate the flexibility of the shake table, all of which led to significant improvements to the analytical model. The link slab and notches were modeled with beam-column elements, providing the stiffening of the web wall observed in the test. The gravity columns contributed to the lateral resistance by developing axial tension and compression in the columns located at opposite ends of the web wall, thereby creating a moment couple. The axial loads in the columns were controlled by the 3D deformation of the floor slabs. A 3D ANSYS analysis determined an effective slab width of 11.5 times the slab thickness, which was used to define the behavior of a beam-column element at each floor level to capture the corresponding effect in the 2D OpenSees model. The improved model remains simple and easy to construct, while giving accurate simulation of the structural response.

The conclusions drawn from the analysis of a large system such as the test building studied herein are:

- Simple, computationally efficient 2D models with fiber sections that satisfactorily account for any 3D effect are sufficient to predict the response of concrete wall buildings subjected to unidirectional earthquake motions. In this study, the effect that the floor slabs had on the axial load of the gravity columns was investigated using a 3D ANSYS model, but such an effort will not be needed if an effective floor slab width needed to account for the effect in the 2D model is known.
- Inclusion of the gravity columns, link slab, and table flexibility were required to accurately capture the response of the structure to the earthquake input motions. Neglecting these components in the original model significantly affected the ability of the model to predict the dynamic response of the building.
- The gravity columns contributed significantly to the overturning moment in the structure. The couple generated by the axial load in the columns contributed 10–24% to the overturning moment. The contribution of the gravity columns generally increased as the intensity of the earthquake motions increased.
- The time-history responses for the top-floor displacement, base overturning moment, and top-floor acceleration were well predicted by the improved 2D model for EQ1, EQ2, and EQ4 motions. The analysis gave results within 5% of the measured values for displacements while the base overturning moments and top-floor acceleration peak values were within 10–15%.
- When subjected to input motions EQ1, EQ2, and EQ4, the improved 2D model gave results that were within 5–15% of the envelope for displacement, inter-story drift, overturning moment, and story shear forces.
- Under input motion EQ3, the discrepancies between the analytical responses and the measured values were as large as 25%. This was due to EQ3 having a similar

peak intensity to EQ2, which made the EQ3 response of the test building to be dependent heavily on the unloading and reloading behavior of the material models used in the analysis.

- Despite the building being designed as a flexible structure, the earthquake analysis of the test building did not produce excessive floor displacements or unacceptably large inter-story drift ratios, which is encouraging and consistent with the test observations.

The participation in the blind prediction and follow up analysis of the seven-story building provided a number of lessons about simulating the response of a complex system. These lessons are:

- Although gravity load resisting systems are routinely ignored in the seismic design and analysis of structures, they can significantly contribute to the lateral load resistance of a building. This situation may be expected if gravity columns are subjected to axial forces resulting from their interaction with the floor slabs during lateral movement of the building, enabling moment couples to be generated. Since the distance between gravity columns is typically large, the resulting couple will be significant and should not be ignored.
- In dynamic analysis of concrete buildings, a 5% viscous damping is routinely assumed. At very low intensity of shaking, it was reported that the test building exhibited a damping ratio in the range of 2–6%. However, it appears that for a concrete building with almost no non structural elements and flexural cracking limited to lower stories of the building, a significantly lower viscous damping ratio in the range of 0.3–1.0% should be expected.
- Viscous damping proportional to tangent stiffness is preferred over Rayleigh damping for dynamic analysis of concrete buildings designed to respond nonlinearly. This is because it allows the viscous damping to decline as hysteretic damping increases. This follows the recommendation of Priestley and Grant [2004] regarding viscous damping in concrete structures.
- Accurate representation of the material response envelopes likely leads to satisfactory peak response of the structure subjected to earthquake loads that demand the structure to respond in a virgin territory. However, accurate representation of the unloading and reloading paths of the models used for the material and shear behavior become critical for assessing the performance of a structure subjected to earthquake motions that do not take the structure significantly into a virgin territory. This scenario is expected when predicting response of a structure to aftershocks following its response to the main earthquake event.

Acknowledgments

The study presented in this article was undertaken as part of a PreNEESR project, supported by the National Science Foundation through Grant No. CMS-0324559. The authors gratefully acknowledge the support of Drs. S. McCabe, D. Foutch, and M. P. Singh, who have served as program directors for this grant. The authors would also like to thank Silvia Mazzoni, Frank Mckenna, Gregry Fenves, and PEER for creating OpenSees and providing guidance and assistance to users of the program. Finally, the authors would like to thank NEES-UCSD for sharing the data from the seven-story building test and hosting the NEES/UCSD Seminar on Analytical Modeling of Reinforced Concrete Walls

for Earthquake Resistance. Any opinions, findings, and conclusions or recommendations expressed in this material are those of the authors and do not necessarily reflect the views of NSF.

References

- Barbosa, A. F. and Ribeiro, G. O. [1998] "Analysis of reinforced concrete structures using ANSYS nonlinear concrete model," in *Computational Mechanics: New Trends and Applications*, eds., S. Idelsohn, E. Onat, and E. Dvorkin, CIMNE, Barcelona, Spain pp. 1–7.
- Brueggen, B., Waugh, J., Aaleti, S., Johnson, B., French, C., Sritharan, S., and Nakaki, S. [2007] "Tests of structural walls to determine deformation contributions of interest for performance based design," *Proc. of the 2007 Structures Congress*, American Society of Civil Engineers, Reston, VA.
- Hsu, T. C. [1993] *Unified Theory of Reinforced Concrete*, CRC Press, Boca Raton, FL.
- Kelly, T. [2007] "A blind prediction test of nonlinear analysis procedures for reinforced concrete shear walls," *New Zealand Society for Earthquake Engineering Bulletin* **40**(3), 142–159.
- Mander, J. B., Priestley, M. J. N., and Park, R. [1988] "Theoretical stress-strain model for confined concrete," *Journal of Structural Engineering* **114**(8), 1804–1826.
- Massone, L. M. and Wallace, J. W. [2004] "Load deformation response of slender reinforced concrete walls," *ACI Structural Journal* **101**(1), 103–113.
- Mazzoni, S., McKenna, F., Scott, M. H., and Fenves, G. L. [2004] "Open system for earthquake engineering simulation," *Pacific Earthquake Engineering Research Center*, University of California, Berkeley California, Ver. 1.6.0.
- Moaveni, B., He, X., Conte, J. P., and Restrepo, J. I. [2006] "System identification of a seven-story reinforced concrete shear wall building slice tested on the UCSD-NEES shake table," *NEES-UCSD Workshop on the Analytical Model of Reinforced Concrete Walls*, San Diego, CA.
- NEES7Story [2006] NEES @ UCSD Seven Story Building-Slice Earthquake Blind Prediction Contest. <http://nees.ucsd.edu/7story.html>; accessed June 13, 2007.
- Neuenhofer, A. and Filippou, F. C. [1997] "Evaluation of nonlinear frame finite-element models," *ASCE Journal of Structural Engineering* **123**(7), 958–966.
- Oesterle, R., Aristizabal-Ochoa, J., Fiorato, A., Russel, H., and Corley, W. [1979] "Earthquake resistant structural walls – tests of isolated walls – Phase II," *Report to the National Science Foundation*, Construction Technology Laboratories, Portland Cement Association, Skokie, IL.
- Panagiotou, M. and Restrepo, J. [2006] "Model calibration for the UCSD 7-story building slice", *NEES-UCSD Workshop on the Analytical Model of Reinforced Concrete Walls*, San Diego, CA.
- Park, R. and Paulay, T. [1975] *Reinforced Concrete Structures*, John Wiley & Sons, New York.
- Restrepo, J. [2006] "Proceedings of the NEES/UCSD workshop analytical model of reinforced concrete walls", *NEES-UCSD Workshop on the Analytical Model of Reinforced Concrete Walls*, San Diego, CA.
- Sritharan, S., Zhao, J., Waugh, J., and Govindarasu, M. [2005] "Nonrectangular concrete walls under multi-directional loads – analytical simulation and remote participation in experimental research," *Proc. of the First US-Portugal International Workshop on Grand Challenges in Earthquake Engineering*, Lamego, Portugal.
- Swanson Analysis System [1992] "Ansys User's Manual (for Ansys Revision 5.0) Part IV: Theory," *Swanson Analysis Systems Houston, PA*.
- Thomsen, J. H. and Wallace, J. W. [1995] "Displacement based design of RC structural walls: an experimental investigation of walls with rectangular and T-shaped cross-sections," *Report to the National Science Foundation*, Department of Civil Engineering, Clarkson University, Potsdam, NY.
- Waugh, J. and Sritharan, S. [2006] "Description of analysis model used for predicting behavior of 7-story test building," *NEES-UCSD Workshop on the Analytical Model of Reinforced Concrete Walls*, San Diego, CA.
- Zhao, J. and Sritharan, S. [2007] "Modeling of strain penetration effects in fiber-based analysis of reinforced concrete structures," *ACI Structural Journal* **104**(2), 133–141.